

A photometric study of NSVS 7453183: a probable quadruple system with long-term surface activity

L. Šmelcer,^{1,7} M. Wolf,^{2*} H. Kučáková,^{2,3,4,7} P. Zasche,² J. Kára,² K. Hornoch,³ M. Zejda,⁵ and R.F. Auer^{6,7}

¹Valašské Meziříčí Observatory, Vsetínská 78, CZ-757 01 Valašské Meziříčí, Czech Republic

²Astronomical Institute, Faculty of Mathematics and Physics, Charles University Prague, V Holešovičkách 2, CZ-180 00 Praha 8, Czech Republic

³Astronomical Institute, Academy of Sciences, Fričova 298, CZ-251 65 Ondřejov, Czech Republic

⁴Research Centre for Theoretical Physics and Astrophysics, Institute of Physics, Silesian University in Opava, Bezručovo nám. 13, CZ-746 01 Opava, Czech Republic

⁵Department of Theoretical Physics and Astrophysics, Masaryk University, Kotlářská 2, CZ-611 37 Brno, Czech Republic

⁶South-Moravian Observatory, Chudčice 273, CZ-64771 Veverská Bítýška, Czech Republic

⁷Czech Astronomical Society, Variable Star and Exoplanet Section, Vídeňská 1056, CZ-142 00 Praha 4, Czech Republic

Accepted 2023 January 3. Received 2022 December 6; in original form 2022 October 11

ABSTRACT

The VRC light curves were regularly measured for the eclipsing binary NSVS 7453183 as a part of our long-term observational project for studying of low-mass eclipsing binaries with a short orbital period and surface activity. The TESS light curve solution in PHOEBE results to the detached configuration, where the temperature of primary component was adopted to $T_1 = 4300$ K according to the SED approximation. It gives us $T_2 = 4080 \pm 100$ K for the secondary component. The spectral type of the primary component was estimated to be K6 and the photometric mass ratio was derived $q = 0.86$. We confirm presence of the third body in this system, a stellar companion with a minimal mass $0.33 M_\odot$ orbiting the eclipsing pair with a short period about 425 days, and propose the next, fourth body with a longer orbiting period of about 12 years, probably a brown dwarf with the minimal mass of $50 M_{\text{Jup}}$. The hierarchical structure $((1+1)+1)+1$ of this quadruple system is assumed. Characteristics and temporal variations of the dark region on the surface of the primary component were estimated. The average migration speed of about 10 deg/month was found during years 2020–2022.

Key words: binaries: close – binaries: eclipsing – binaries: low-mass – stars: activity – stars: fundamental parameters – stars: individual: NSVS 7453183

1 INTRODUCTION

The most common and frequent stars in our Galaxy are late-type and low-mass stars, dwarfs with masses below $1.0 M_\odot$. Moreover, current observations of low-mass stars show a discrepancy between estimated and modeled parameters, where the models give 5–10 % smaller radii and higher temperatures than observations (Chabrier & Baraffe 2000; Morales et al. 2010; Mann et al. 2015). Many eclipsing binaries (EB) display a periodic variation of their mid-eclipse times caused by various phenomena. One is the light-time effect (LITE) associated with the presence of a third body orbiting the eclipsing pair (Irwin 1952, 1959), the second alternative is magnetically-induced gravitational modulation caused by an active star in the system (Aplegate 1992). The fundamental properties of late-type stars in EB were recently summarized by Morales et al. (2022), who confirmed the above mentioned discrepancy and emphasize importance of low-mass stars to precision of our stellar evolution models.

Like our Sun, the low-mass stars are also affected by chromospheric activity caused by a strong magnetic field. This variable activity has been frequently observed as flares, dark or bright spots on the surface and plays important role for determination of precise physical parameters, esp. their radii and temperatures. For the first

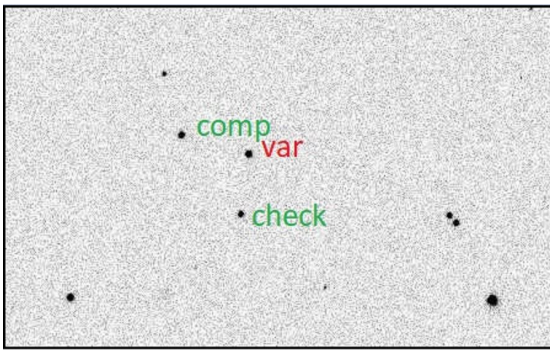
time, the spot activity in stars was announced by Kron (1950) who detected the sinusoid-like variations in the light curve of eclipsing binary YY Gem.

The low-mass eclipsing binary NSVS 07453183 (in SIMBAD also as NSVS 07446320, 2MASS J09161228+3615335, hereafter N745) is rather faint northern object with a short orbital period of about 9 hours. Its variability was discovered by McIntyre & Shaw (2005) using the publicly available *Northern Sky Variability Survey* (NSVS, Wozniak et al. 2004). First photometric solution of N745 was presented by Coughlin & Shaw (2007) who derived preliminary masses and dimensions of components ($M_1 = 0.68$, $M_2 = 0.73 M_\odot$, $R_1 = 0.72$, $R_2 = 0.79 R_\odot$). Using the program Eclipsing Light Curves (ELC) they also found two spots on the surface of the hotter and more massive component with longitudes -33 and $+17$ deg and angular radii 100 and 9.3 deg, respectively. Their analysis supports the current findings that low-mass stars have greater radii than models predict, most likely due to the presence of strong magnetic fields. Next BVR photometry and period analysis of N745 were presented by Zhang et al. (2014), who also detected a flare-like event. Later, the period analyses of N745 was presented by Wolf et al. (2016). They found a probable third body in this system, a stellar companion with a minimal mass $0.41 M_\odot$ orbiting the eclipsing pair with a short period of about 418 days. The following linear ephemeris were proposed in that paper for the current use:

* E-mail: marek.wolf@mff.cuni.cz

Table 1. GAIA DR2 astrometric and photometric data on N745.

Parameter	Value
α_{2000} [h m s]	09 16 12.27
δ_{2000} [d m s]	+36 15 33.5
pm α [mas/yr]	-28.52 ± 0.07
pm δ [mas/yr]	-11.75 ± 0.06
parallax π [mas]	3.311 ± 0.074
V [mag]	13.012 ± 0.038
G [mag]	13.000 ± 0.0074
BP [mag]	13.629 ± 0.0258
RP [mag]	12.287 ± 0.0207
J [mag]	11.300 ± 0.022
H [mag]	10.740 ± 0.016
K [mag]	10.608 ± 0.016

**Figure 1.** The finding chart of N745, the dimensions are approx. 8×5 arcmin, north is up. The position of variable, comparison and check stars are denoted.

$$\text{Pri.Min.} = \text{HJD } 24\,53456.85994 + 0^{\text{d}}.36696751 \cdot E.$$

GAIA DR2 astrometric and photometric data on N745 are summarized in Table 1 (Gaia Collaboration et al. 2020). The distance to the system was derived to be $d = 314$ pc. To our knowledge, no modern photometric or spectroscopic analyses of this short-period eclipsing binary exists so far.

The paper is organized as follows: in Section 2 we present the observational data used in the analysis. The orbital period study and the light-time effect are described in Section 3. The photometric solution is given in Section 4 and discussion of the flare activity of N745 is given in Section 5. The paper is finished by discussion (Section 6) and our conclusions are summarized in Section 7.

2 OBSERVATIONS

In this section, we describe the properties and reduction process of our observations of N745. We present our long-term ground-based photometry (2.1), TESS photometry (2.2), and an older optical spectrum from Keck observatory (2.3).

2.1 Ground-based photometry

Since 2009 the time-resolved CCD photometry of N745 mostly during eclipses has been regularly obtained at several observatories in Czech Republic. The focused photometric campaign has been initiated in April 2019 to determine the eruption activity and flare

Table 2. Coordinates of selected stars in the field of N745, see Figure 1.

Object	α_{2000} [h:m:s]	δ_{2000} [d:m:s]	V [mag]	USNO-B1.0
N745 (var)	09 16 12.27	+36 15 33.51	13.0	1262-0172833
comparison	09 16 17.00	+36 15 49.41	13.25	1262-0172847
check	09 16 12.74	+36 14 42.27	13.91	1262-0172837

frequency and to derive their characterization and relatively large amount of photometric data was obtained.

- Most observations in our campaign were obtained at Valašské Meziříčí observatory, Czech Republic, in 2014, and more systematically from January 2019 to November 2022. Three different telescopes, CCD camera and filters were used regularly each clear night: Celestron SCT 280/1765, camera MII G2-4000 with filter B, Sky-Watcher NWT 254/1200, camera CCD QHY 174 and filter C (clear), and Celestron SCT 355/2460, camera MII G2-1600 with filter V.

- Since 2009 semi-regular observations were performed at Ondřejov observatory, Czech Republic, where the Mayer 0.65-m ($f/3.6$) reflecting telescope with the CCD camera MII G2-3200 and VR photometric filters were used.

- Important additional photometry was obtained at Masaryk University Observatory in Brno, Czech Republic, during three separate epochs: in March/April 2010, February/March 2020 and April/May 2022. The 0.60-m reflecting telescope with the CCD camera MII G4-16000 and VR photometric filters were included.

- Supplementary photometry was obtained at South-Moravian Observatory of R.F.A. in Veverská Bítýška, Czech Republic, where 0.2-m ($f/4$) Newtonian telescope with the CCD camera MII G2-1600 and C (clear) filter were used during March/April 2021.

The CCD observations were reduced in a standard way. The C-MUNIPACK¹, a synthetic aperture photometry software, was routinely used for our time-series photometry. At Ondřejov the APHOT (Pravec et al. 1994), synthetic aperture photometry and astrometry software were used for time series. Time-series were constructed by computing the magnitude difference between the variable and a nearby comparison and check stars, see Fig. 1 and Table 2, the heliocentric correction was applied. The uncertainties of photometric measurements at smaller telescopes were always about 0.01 – 0.02 mag. Computers at the 65-cm telescope are synchronized using a time-server provided by <http://ntp.cesnet.cz> every two minutes. These corrections are usually in order of 10^{-3} seconds. Together at all observatories it was obtained nearly 60 000 frames in V, R, I and C filters.

2.2 TESS photometry

As a northern object N745 was measured twice by the *Transiting Exoplanet Survey Satellite* (TESS, Ricker et al. (2015)) in Sector 21 (Jan/Feb 2020) and Sector 48 (Jan/Feb 2022). We used the MAST² database to download the photometric time-series. These high-quality light curves allowed us the precise mid-eclipse time determination as well as modeling of the system.

¹ Package of software utilities for reducing astronomy CCD images, current version 2.1.31, available at <http://c-munipack.sourceforge.net/>

² MAST: Barbara A. Mikulski Archive for Space Telescopes, <https://mast.stsci.edu/portal/Mashup/Clients/Mast/Portal.html>

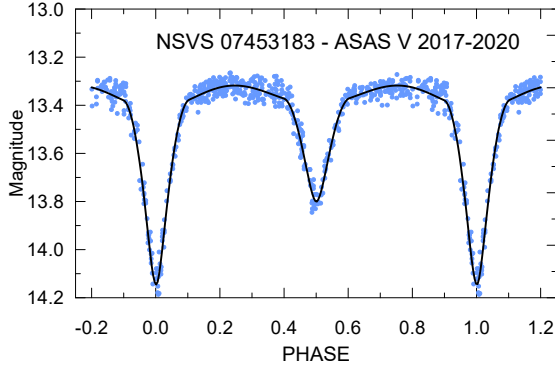


Figure 2. For illustration, the mean ASAS SN-V light curve of N745 obtained during 2017-2020 and its solution in PHOEBE. Due to relatively large scatter of data no spots on the surface of both components were employed.

The new times of primary and secondary minima and their uncertainties were generally determined by fitting the light curve by Gaussians or polynomials of the third or fourth order; we used the least-squares method. They are listed in Table 3 and 4, where epochs were computed according to the following improved linear ephemeris:

$$\text{Pri. Min.} = \text{BJD } 24\,53456.8597 + 0^{\text{d}}366967684 \cdot E.$$

Because the TESS data are provided in the Barycentric Julian Date Dynamical Time (BJD_{TDB}), all our times in Table 3 were first transformed to this time scale using the often used Time Utilities of Ohio State University³ (Eastman et al. 2010).

N745 is also included in the ASAS-SN database (Shappee et al. 2014) as an object ASASSN-V J091612.17 +361533.7. Unfortunately, the large scatter of these data does not allow us to determine the reliable solution of the light curve nor precise parameters of possible surface spots. The ASASSN-V light curve of N745 obtained during 2017-2020 is plotted in Fig. 2.

2.3 Keck spectrum

One spectrum of N745 obtained on January 1, 2012, is immediately available in the Keck Observatory Archive (KOA)⁴. The HIRES spectrograph with 180 sec exposure time was used. The whole calibrated spectrum covers the wavelengths 4450 – 8910 Å and clearly shows the emission lines of the Balmer series of hydrogen (see Fig. 3 for illustration).

3 ORBITAL PERIOD STUDY

The period changes of N745 were studied in detail last time in Wolf et al. (2016). To confirm our previous finding we continued in monitoring of eclipses to extend the $O-C$ diagram and to reveal the nature of the rapid period changes. Based on the current data set extended by seven years of continuous measurements we propose a quadruple system with remarkable surface activity, where the eclipsing pair is orbiting by two additional bodies. Such a long-term project was possible only with the help of several advanced amateur observers.

³ <http://astrutils.astronomy.ohio-state.edu/time/>

⁴ KOA Data Access Service - v18.5, <https://koa.ipac.caltech.edu/cgi-bin/KOA/nph-KOAlogin>

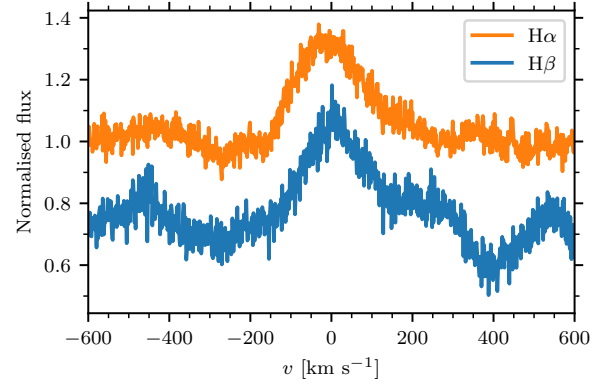


Figure 3. The broad hydrogen H α and H β line profiles of N745 obtained at Keck Observatory in January 2012.

3.1 Light-time effect

The light-time effect (LITE) in N745 were studied traditionally by means of an $O-C$ diagram (or ETV curve) analysis. As has been proven many times in the past, this simple and effective technique is a very powerful tool to investigate the multiplicity of stellar systems. For a detailed description of LITE analyses see the original papers of Irwin (1952, 1959); Frieboes-Conde & Herczeg (1973); Mayer (1990); Sterken (2005). The basic fitting equations are as follows. The observed deviations of mid-eclipse times $(O-C)_{\text{obs}}$ from the linear ephemeris is given by a superposition caused by a third and fourth bodies:

$$(O-C)_{\text{obs}} = (O-C)_{\text{LITE},3} + (O-C)_{\text{LITE},4}.$$

The light-travel time caused by a third body is given by

$$(O-C)_3 = \frac{A_3}{\sqrt{1 - e_3^2 \cos^2 \omega_3}} \left[\frac{1 - e_3^2}{1 + e_3 \cos v_3} \sin(v_3 + \omega_3) + e_3 \sin \omega_3 \right], \quad (1)$$

where e_3 is the eccentricity of the third-body orbit, ω_3 the longitude of periastron and v_3 the true anomaly of the third body. Similarly for the fourth body

$$(O-C)_4 = \frac{A_4}{\sqrt{1 - e_4^2 \cos^2 \omega_4}} \left[\frac{1 - e_4^2}{1 + e_4 \cos v_4} \sin(v_4 + \omega_4) + e_4 \sin \omega_4 \right], \quad (2)$$

where e_4 is the eccentricity of the fourth-body orbit, ω_4 the longitude of periastron and v_4 the true anomaly of the fourth body. The observed semi-amplitudes A_3 and A_4 of the light-time curves (in days) are

$$A_3 = \frac{a_{12,3} \sin i_3}{173.15} \sqrt{1 - e_3^2 \cos^2 \omega_3}, \quad (3)$$

$$A_4 = \frac{a_{12,4} \sin i_4}{173.15} \sqrt{1 - e_4^2 \cos^2 \omega_4}, \quad (4)$$

where $a_{12,3}$ and $a_{12,4}$ are the semi-major axes of the relative orbits of the eclipsing pair around the common center of mass (in AU), i_3

Table 3. New ground-based times of primary and secondary eclipses of N745 obtained since January 2019.

BJD -24 00000	Error [day]	Filters	Epoch	O	BJD -24 00000	Error [day]	Filters	Epoch	O	BJD -24 00000	Error [day]	Fil.	Epoch	O
58503.39892	0.00005	R	13752.0	2	59269.44233	0.0003	C,V,R	15839.5	1	59595.49524	0.0001	C	16728.0	1
58506.3332	0.0003	C	13760.0	1	59269.62762	0.0002	C,V,R	15840.0	1	59599.34786	0.0002	C	16738.5	1
58590.3722	0.0001	C	13989.0	1	59271.64319	0.0001	V,R	15845.5	2	59624.30126	0.0001	C,R	16806.5	1
58591.4732	0.0001	C	13992.0	1	59275.31363	0.0003	C,B,V,R,I	15855.5	1	59624.48479	0.0001	C,R	16807.0	1
58888.53286	0.0002	V,R	14801.5	4	59276.41449	0.0002	C,B,V,R,I	15858.5	1	59625.40217	0.0001	C	16809.5	1
58926.51274	0.0002	V,R	14905.0	4	59276.59977	0.0003	C,B,V,R,I	15859.0	1	59625.58609	0.0001	C	16810.0	1
58935.31922	0.0001	R	14929.0	2	59281.37048	0.0001	C,V,R	15872.0	1	59628.33789	0.0001	C	16817.5	1
58947.43041	0.0001	C	14962.0	1	59281.55226	0.0001	C,V,R	15872.5	1	59639.53054	0.0001	C	16848.0	1
58948.34981	0.0001	C	14964.5	1	59284.30628	0.0001	C,V,R	15880.0	1	59640.26458	0.0001	C	16850.0	1
58951.53129	0.0001	C,V	14973.0	1	59284.48818	0.0002	C,V,R	15880.5	1	59640.44734	0.0001	C	16850.5	1
58952.38635	0.0001	C,B,V	14975.5	1	59286.32282	0.0001	C,V,R	15885.5	1	59641.36568	0.0001	C	16853.0	1
58955.32222	0.0002	C,B,V	14983.5	1	59286.50824	0.0001	C	15886.0	1	59641.54840	0.0001	C	16853.5	1
58955.50421	0.0002	C,B,V	14984.0	1	59294.39634	0.0002	C,V,R	15907.5	1	59647.41969	0.0001	C	16869.5	1
58956.42338	0.0001	C,B,V	14986.5	1	59294.58117	0.0001	C,R	15908.0	1	59648.33769	0.0001	C	16872.0	1
58959.35896	0.0002	C,B,V	14994.5	1	59299.35240	0.0001	C	15921.0	1	59649.43873	0.0001	C	16875.0	1
58960.45965	0.0002	C,B,V	14997.5	1	59300.26863	0.0001	C	15923.5	1	59649.62123	0.0001	C	16875.5	1
58961.37575	0.0001	B,V	15000.0	1	59300.45318	0.0001	C	15924.0	1	59650.35565	0.0001	C	16877.5	1
58962.47694	0.0002	B,V	15003.0	1	59304.30487	0.0001	C	15924.5	1	59650.53970	0.0001	C	16878.0	1
58963.39574	0.0002	C,B,V	15005.5	1	59304.48998	0.0001	C	15935.0	1	59651.27353	0.0001	C	16880.0	1
58966.33150	0.0002	B,V	15013.5	1	59304.30386	0.0003	C	15934.5	3	59651.45660	0.0001	C	16880.5	1
58967.43226	0.0002	C,B,V	15016.5	1	59304.48892	0.0003	C	15935.0	3	59651.64037	0.0001	C	16881.0	1
58968.34814	0.0001	C,B,V	15019.0	1	59305.40558	0.0001	C	15937.5	1	59652.37491	0.0001	C	16883.0	1
58990.36657	0.0001	C,V	15079.0	1	59309.44237	0.0001	C	15948.5	1	59652.55782	0.0002	C	16883.5	1
59127.61190	0.0001	V,R,I	15453.0	1	59311.27770	0.0001	C	15953.5	1	59657.32840	0.0001	C	16896.5	1
59161.55480	0.0002	V,R,I	15545.5	1	59311.46251	0.0001	C	15954.0	1	59657.51181	0.0001	C	16897.0	1
59172.56298	0.0003	B,V,R,I	15575.5	1	59313.29747	0.0001	C	15959.0	1	59659.34686	0.0001	C	16902.0	1
59174.58364	0.0001	C	15581.0	1	59313.47910	0.0001	C	15959.5	1	59659.52992	0.0001	C	16902.5	1
59175.49955	0.0001	C	15583.5	1	59313.29643	0.0003	C	15959.0	3	59660.44757	0.0001	C	16905.0	1
59178.43494	0.0003	B,V,R,I	15591.5	1	59328.34354	0.0001	C	16000.0	1	59661.36466	0.0001	C	16907.5	1
59178.62044	0.0002	B,V,R,I	15592.0	1	59330.35988	0.0001	C	16005.5	1	59661.54864	0.0001	C	16908.0	1
59184.49144	0.0001	V,R	15608.0	1	59332.38020	0.0001	C	16011.0	1	59662.46558	0.0001	C	16910.5	1
59184.67316	0.0001	V,R	15608.5	1	59333.29582	0.0001	C	16013.5	1	59663.38343	0.0001	C	16913.0	1
59185.40729	0.0003	C,V,R	15610.5	1	59333.48106	0.0001	C	16014.0	1	59663.56644	0.0001	C	16913.5	1
59185.59294	0.0001	C,V,R	15611.0	1	59338.43333	0.0001	C	16027.5	1	59666.31891	0.0001	C	16921.0	1
59192.56481	0.0001	C,V,R	15630.0	1	59343.38965	0.0001	C	16041.0	1	59666.50212	0.0001	C	16921.5	1
59210.36019	0.0003	V,R	15678.5	1	59344.30559	0.0002	C	16043.5	1	59681.36442	0.0001	C	16962.0	1
59210.54617	0.0001	V,R	15679.0	1	59344.40916	0.0001	C	16044.0	1	59681.54797	0.0001	C	16962.5	1
59225.40604	0.0002	C,V,R	15719.5	1	59345.40593	0.0001	C	16046.5	1	59682.28176	0.0002	C	16964.5	1
59225.59153	0.0001	C	15720.0	1	59368.34349	0.0001	C	16109.0	1	59682.46553	0.0001	C	16965.0	1
59242.65322	0.0002	C,V,R,I	15766.5	1	59370.36039	0.0001	C	16114.5	1	59684.30031	0.0001	C	16970.0	1
59260.26792	0.0003	B,V,R,I	15814.5	1	59488.52565	0.0001	C	16436.5	1	59689.43762	0.0001	C	16984.0	1
59260.45347	0.0002	B,V,R,I	15815.0	1	59496.59883	0.0001	C	16458.5	1	59691.45616	0.0002	C	16989.5	1
59260.63513	0.0003	B,V,R,I	15815.5	1	59512.56291	0.0001	C,R	16502.0	1	59698.42869	0.0001	C	17008.5	1
59264.30463	0.0002	C,B,V,R,I	15825.5	1	59523.57177	0.0001	C	16532.0	1	59699.34586	0.0001	C	17011.0	1
59265.40487	0.0001	V	15828.5	2	59543.56987	0.0001	C	16586.5	1	59710.35487	0.0001	C	17041.0	1
59265.40474	0.0001	R	15828.5	2	59552.56098	0.0001	C	16611.0	1	59711.45596	0.0001	C	17044.0	1
59266.32367	0.0001	V	15831.0	2	59586.32110	0.0001	C	16703.0	1	59712.37331	0.0001	C,R	17046.5	1
59266.32386	0.0001	R	15831.0	2	59586.50400	0.0001	C	16703.5	1	59719.34562	0.0001	C	17065.5	1
59267.42574	0.0002	C,B,V,R,I	15834.0	1	59586.68804	0.0001	C	16704.0	1	59891.63920	0.0001	R	17535.0	1
59267.60711	0.0002	C,B,V,R,I	15834.5	1	59587.42214	0.0001	C	16706.0	1	59896.59414	0.0002	R	17548.5	1
59268.34107	0.0002	C,V,R,I	15836.5	1	59587.60504	0.0001	C	16706.5	1	59913.47404	0.0002	R	17594.5	1
59269.26049	0.0002	C,V,R	15839.0	1	59595.31112	0.0001	C	16727.5	1					

Notes: O (observatory): 1 - Valašské Meziříčí, 2 - Ondřejov, 3 - Veverská Bítýška, 4 - Brno

and i_4 are inclinations of the third- and fourth body orbits. There are following independent variables to be determined in this procedure:

($A_3, P_3, T_3, e_3, \omega_3$) for the LITE of the third body, and

($A_4, P_4, T_4, e_4, \omega_4$) for the LITE of the fourth body,

where P_3 and P_4 are orbital periods of the third and fourth bodies,

T_3 and T_4 are times of periastron and e_3 and e_4 are eccentricities of their respective orbits. The linear ephemeris (T_0, P_S) of the eclipsing pair are a part of this set of 12 unknown parameters.

The period analysis of N745 was performed using all available

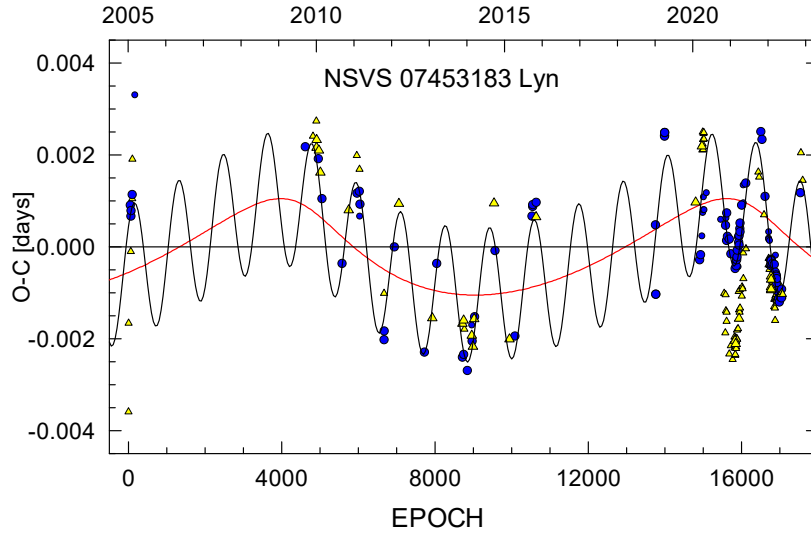


Figure 4. The complete $O-C$ diagram for the times of minimum of N745 since its discovery in 2005. The individual primary and secondary CCD minima obtained are denoted by blue circles and yellow triangles, respectively. Larger symbols correspond to the precise CCD measurements, which were used in our calculation of the LITE. The black sinusoidal curve represents the LITE with the short period of about 425 days. The red curve denotes long-term change with a period of 12 years caused probably by a fourth orbiting body.

Table 4. New times of primary and secondary eclipses of N745 based on the TESS photometry, Sector 48, January 2022.

BJD -24 00000	Epoch
59609.43960	16766.0
59609.80643	16767.0
59609.98971	16767.5
59610.17350	16768.0
59610.35645	16768.5
59610.54048	16769.0
59610.72336	16769.5
59610.90737	16770.0
59611.09031	16770.5
59611.27434	16771.0
59611.45730	16771.5
59611.64139	16772.0
59611.82448	16772.5
59612.00834	16773.0

mid-eclipse times found in the literature ($O-C$ gateway⁵, Paschke & Brát 2006) and primarily by our long-measured series of mid-eclipse times. Besides those minima given in Tables 3 and 4, we used previous times of minimum obtained by McIntyre & Shaw (2005), Zhang et al. (2014) (their Table 4), and Wolf et al. (2016) (their Table A.3). A total of 227 precise CCD times including 110 secondary eclipses were used for the analysis. The least-squares method was applied and resulting LITE parameters and their internal errors of the fit are given in Table 5 (in parenthesis). The historical $O-C$ diagram since discovery N745 as variable star is plotted in Fig. 4. It is clearly visible that mid-eclipse times do not follow a simple linear ephemeris during past 15 years. The current $O-C$ diagrams in detail is shown in Fig. 5.

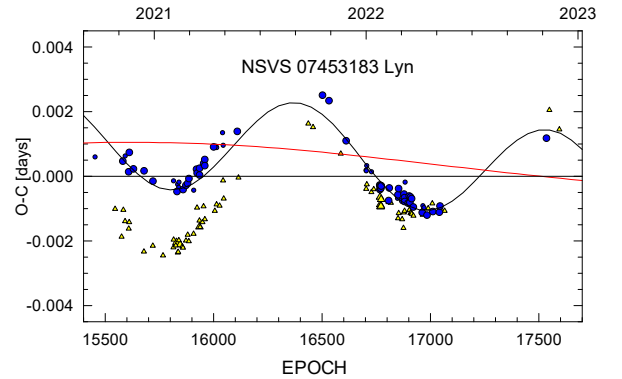


Figure 5. The $O-C$ diagram of N745 in detail for minima obtained during two last seasons in 2021 and 2022. The black sinusoidal curve fitting the primary minima denotes the LITE with short period of 425 days, the red curve corresponds to LITE of the fourth body with period of 12 years. Note, that the secondary minima (yellow triangles) have a different course modulated by short-period LITE.

Assuming a coplanar orbit of the third and fourth bodies ($i_3, i_4 \approx 90^\circ$) and the total mass of the eclipsing pair $M_1 + M_2 \approx 1.45 M_\odot$ (Coughlin & Shaw 2007), we can estimate a lower limit for the mass of the third and fourth components, $M_{3,\min}$ and $M_{4,\min}$. This value, as well as the mass functions $f(m)$, and the amplitudes of the systemic radial velocity K_3 and K_4 are also given in Table 5. The probable third component may be a main-sequence star of a spectral type M3 with a bolometric magnitude of about +9.2 mag (Pecaut & Mamajek 2013)⁶ produces a detectable third light of $L_3 \approx 6\%$. This is in good agreement with the solution of TESS light curves where the third light of about 7% was found. See Table 7 in Section 4. The possible fourth body may be a brown dwarf with mass about $0.05 M_\odot$, which is practically invisible in the system of two K stars.

⁵ <http://var2.astro.cz/ocgate>

⁶ http://www.pas.rochester.edu/~emamajek/EEM_dwarf_UBVIJHK_colors_Teff.txt

Table 5. The improved LITE elements and the minimal masses of the possible third and fourth bodies.

Parameter	Unit	Value
T_0	BJD	24 53456.8597 (1)
P_s	day	0.366967681 (9)
A_3	days	0.00146 (5)
P_3	days	425.5 (7.8)
P_3	years	1.165 (0.021)
e_3	–	0.0 (fixed)
ω_3	deg	357.4 (1.2)
T_3	JD	24 58930 (10)
$f (M_3)$	M_\odot	0.0120
$M_{3,\min}$	M_\odot	0.33
K_3	km s^{-1}	6.5
$A_{\text{dyn},3}$	days	0.000 05
A_4	days	0.00105 (15)
P_4	days	4271 (350)
P_4	years	11.7 (0.9)
e_4	–	0.40 (0.15)
ω_4	deg	122.6 (2.5)
T_4	JD	24 55138 (30)
$f (M_4)$	M_\odot	0.000 047
$M_{4,\min}$	M_\odot	0.047
K_4	km s^{-1}	0.52
$\Sigma w (O - C)^2$	day^2	$8.5 \cdot 10^{-5}$

We also tested the so-called physical delay, the direct gravitational influence of the third body on the motion of an eclipsing pair. The amplitude of the dynamical contribution of the third body, A_{dyn} , is given by Rappaport et al. (2013) or Borkovits et al. (2016):

$$A_{\text{dyn}} = \frac{3}{8\pi} \frac{M_3}{M_1 + M_2 + M_3} \frac{P_s^2}{P_3} (1 - e_3^2)^{-3/2}$$

and is also listed in Table 5. The value of $A_{\text{dyn},3}$ is in the order of seconds and comparable with the uncertainty of individual mid-eclipse time estimation. Thus the physical delay cannot contribute significantly to observed changes of $O - C$ values.

3.2 Magnetic activity

A possible alternative scenario to the third body and LITE hypothesis assumes the period modulation in binaries connected with magnetic activity of stars. Applegate (1992) proposed a model which explains orbital period modulations as a consequence of the magnetic activity changes of one of the components. According to this model, the component, which has a magnetic activity cycle, can show a period change of $\Delta P/P \approx 10^{-5}$ only.

4 LIGHT CURVE SOLUTION

4.1 Temperature of the primary component

Effective temperatures of binary components are crucial parameters of all photometric models. In absence of direct spectroscopic results we searched available literature. There are several different estimations of temperature found in the current catalogs which are collected in Table 6. For N745 it can be seen a difference over 2000 K.

Table 6. Temperatures of N745 found in different sources.

Source	Temp. [K]	Reference
SIMBAD Sp. type M2	3560	Pecaut & Mamajek (2013)
Regression of stellar T_{eff}	4503	Bai et al. (2019)
TESS Input Catalog	4533	Stassun et al. (2019)
GAIA DR2	4700	Gaia Collaboration et al. (2018)
GAIA DR3	4719	Gaia Collaboration (2022)
Starhorse catalog	5753	Anders et al. (2019)

Removing both extreme values we can obtain the mean value of 4613 ± 200 K.

On the other hand analyzing available photometry by the more robust SED fitting using the Virtual Observatory SED Analyzer (VOSA, Bayo et al. (2008)), we can obtain for black-body radiation of a binary model temperatures $4300 + 4200$ K. Thus we accepted the effective temperature of primary component $T_1 = 4300 \pm 100$ K, which was used in our next light curve modeling. Pecaut & Mamajek (2013) give for this temperature the color index $J - H = 0.60$ mag and the spectral type K6, the GAIA archive and the SIMBAD database present the similar value of $J - H = 0.56$ mag.

4.2 PHOEBE solution

As a first attempt we selected roughly 1500 points of the precise TESS light curves obtained in Sectors 21 and 48, to obtain basic photometric parameters of the system. The wavelength coverage of TESS is about $6000 - 10000$ Å, covering most of the R and I filters. These high quality light curves were analyzed using the well-known PHOEBE code (Prša & Zwitter 2005; Prša et al. 2016), which is based on the Wilson–Devinney algorithm (Wilson & Devinney 1971) and is widely used for modeling the photometric light curves of eclipsing binaries as a standard tool. Because N745 belongs to late-type binaries, we adopted the bolometric albedos and gravity darkening coefficients as $A_1 = A_2 = 0.5$ and $g_1 = g_2 = 0.32$, which corresponds to the convective envelopes (see Lucy (1968)). Synchronous rotation for both components of the system ($F_1 = F_2 = 1$) and a circular orbit ($e = 0$) were assumed. We used the linear cosine limb-darkening law with the coefficients adopted from van Hamme (1993) tables.

The adjustable parameters were the inclination i , the effective temperature of the secondary component T_2 , luminosities L_1, L_2 , dimensionless potentials of both components Ω_1, Ω_2 , the third light L_3 and the characteristics of the dark spot on the primary component (colatitude, longitude, spot radius and temperature factor). The need to include a spot to the final solution was evident in view of the modulation of out-of-eclipse light curves. Because the effective temperature and the radius of a spot are strongly correlated, we assumed that the ratio of spot/star temperatures is close to 0.9 in our analyzes. The fine and coarse grid raster for both components were set to 40.

All additional light curves obtained Ondřejov in 2010, in Brno in 2010 and 2020, in Valašské Meziříčí in 2014 and 2020, and Veverská Bítýška in 2021 were then solved independently to estimate primarily the characteristics of the dark region. Numerous PHOEBE runs in a detached mode using the different setup of initial parameters were evaluated. The results as well as the cost function value were recorded. The final solution was accepted when subsequent iterations did not result in a decrease of the PHOEBE cost function. We also made some preliminary tests placing spot on both components

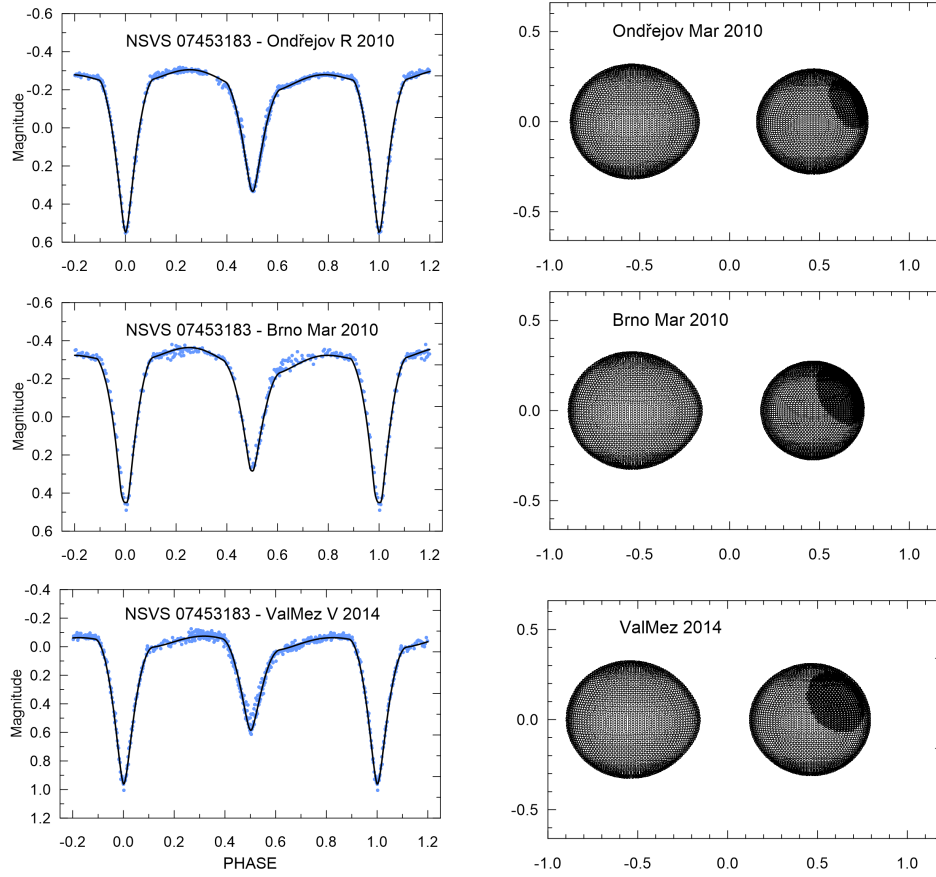


Figure 6. Left: Comparison of light curves of N745 obtained at Ondřejov (top) and Brno (middle) in 2010 and Valašské Meziříčí (bottom) in 2014 and its solution in PHOEBE. Right: The geometrical configuration in phase 0.75. A large dark area on the surface of the primary component is visible.

Table 7. Comparison of photometric solutions of previous authors with our TESS photometric elements of N745, the PHOEBE solution.

Parameter	Primary McIntyre & Shaw (2005)	Secondary	Primary Zhang et al. (2014)	Secondary	Primary TESS 2020	Secondary	Primary TESS 2022	Secondary
i [deg]	84.8(0.1)		84.305(0.113)		82.2(0.5)		81.4(0.5)	
$q = M_2/M_1$	1.05(0.005)		0.601(7)		0.861 (fixed)		0.861 (fixed)	
$T_{1,2}$ [K]	4110(10)	4390(10)	3570 (fixed)	3438(6)	4300 (fixed)	4075(100)	4300 (fixed)	4080(100)
$\Omega_{1,2}$	-	-	4.032(44)	3.156(20)	3.52(12)	3.04(15)	3.52(12)	3.04(15)
r (pole)	-	-	0.2894(37)	0.3006(34)	0.297(5)	0.320(7)	0.297(4)	0.316(6)
r (side)	-	-	0.2953(40)	0.3123(40)	0.305(5)	0.332(8)	0.304(3)	0.328(5)
r (point)	-	-	0.3052(47)	0.3675(108)	0.323(5)	0.377(11)	0.322(4)	0.369(5)
r (back)	-	-	0.3015(44)	0.3375(57)	0.316(4)	0.353(10)	0.315(4)	0.348(6)
L_3 [%]	-	-	-	-	6.4		8.1	

at latitudes of 45 deg, which is the region most affected by spots in low-mass stars (Granzler et al. 2000).

The final light curve solution of TESS data compared with previous results are given in Table 7, where inclination, temperatures, potentials and relative radii of both components are given. The mass ratio was fixed to the value 0.861. The resulting parameters of the dark region on the primary component are given in Table 8.

The computed light curves based on derived parameters are compared with our measurements in Figure 6 and 7. The geometrical representations of N745 in phase 0.75 are displayed on the right side of both figures. The good visibility of dark region on the primary component close to this phase supports possible places of a flare ori-

gin in this area. As one can see, the agreement between the theoretical and observed light curves is relatively good.

5 FLARE ACTIVITY

Stellar flares are sudden events in stellar atmospheres, which eject a hot plasma into surroundings and release a quantum of accumulated magnetic energy. The total released energy in the flares ranges usually from $10^{24} - 10^{27}$ J (Pettersen 1989). We can remind, that the significant eruption activity is well known in several low-mass eclipsing binaries: CM Dra (Lacy 1977; Kim et al. 1997; Nelson

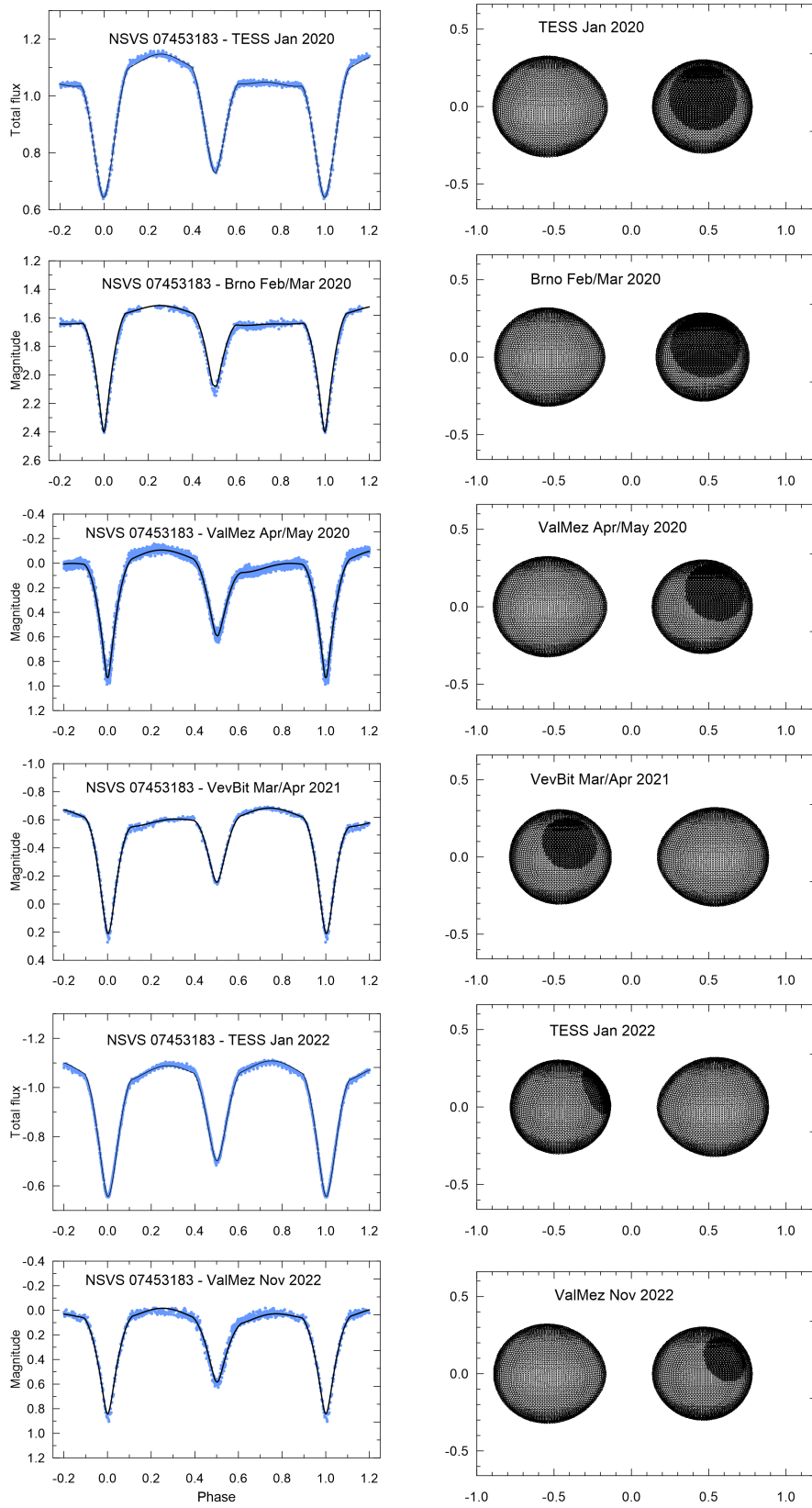


Figure 7. Continuation of Fig. 6. **Left:** Comparison of next six seasonal light curves of N745 in chronological order: data from TESS obtained in January 2020 (top), Brno and Valašské Meziříčí obtained in 2020 (middle), Vevverská Bítýška in April 2021 and next TESS photometry obtained in January 2022 and last curve from Valašské Meziříčí (bottom) and their solutions in PHOEBE. The different shape of the light curve is clearly visible. **Right:** Corresponding geometrical models in phase 0.75 (except the 4th and 5th panel in phase 0.25). The detached configuration with the large dark region persistent on the primary component is distinguishable.

Table 8. Parameters of the surface structure on the primary component of N745 obtained from eight different data sets.

Year	2010	2010	2014	2020	2020	2020	2021	2022	2022
Filters	VR	VR	V	–	R	VR	C	–	R
Observatory	Ond	Brno	ValMez	TESS	Brno	ValMez	VevBit	TESS	ValMez
Colatitude [deg]	65	65	65	60	65	65	65	65	65
Longitude [deg]	145	140	120	85	100	110	295	340	125
Spot radius [deg]	40	40	40	45	50	40	40	30	30
Number of points	490	253	524	1150	431	2900	353	1530	720
Phoebe cost function	900	1200	1350	3150	5650	2900	640	4150	1150

Observatory: Ond = Ondřejov, ValMez = Valašské Meziříčí, VevBit = Veverská Bítýška

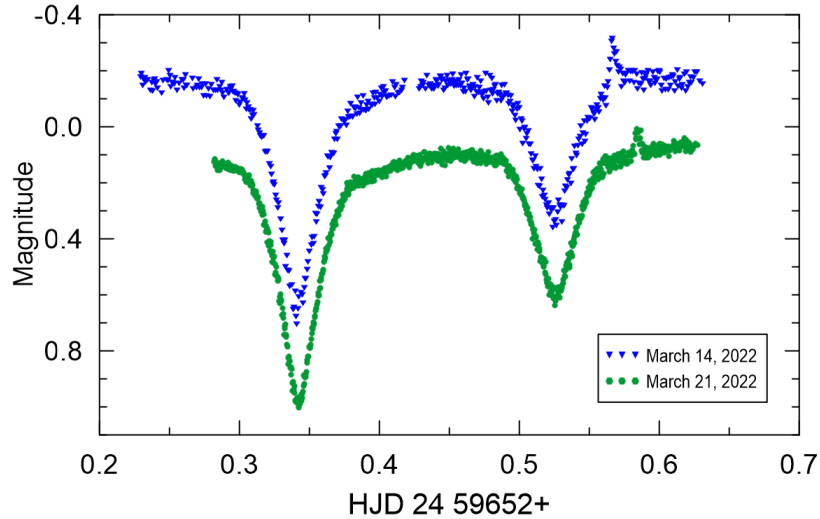


Figure 8. Typical light curves of N745 obtained in clear filter at Valašské Meziříčí observatory on 2022, March 14 (blue triangles) and March 21 (green circles), both showing primary and secondary eclipses followed by a small flare on the similar phase. The amplitude of flares are 0.19 and 0.09 mag, respectively. The light curve obtained on JD 24 59659 was shifted and phased with the previous one for clarity.

& Caton 2007; Kozhevnikova et al. 2009), YY Gem (Doyle et al. 1990), V405 And (Vida et al. 2009), DV Psc (Zhang et al. 2010), NSVS 6550671 (Dimitrov & Kjurkchieva 2010), CU Cnc (Qian et al. 2012), and GJ 3236 (Šmelcer et al. 2017).

Eruption activity of N745 was first reported by Zhang et al. (2014). They observed only one flare event appeared around phase 0.39 on HJD 24 55904.3064. The flare duration was found to be 116 min (phase 0.33–0.55) and the time required for the flare to peak was about 32 min. The amplitudes of the flare were 0.1 mag in V, 0.076 mag in R and 0.05 mag in I band. They also noted, that flare might have been connected to the primary component due to visibility during this phase. Zhang et al. (2014) monitored the object on Dec 8, 2011, and during 26.6 hours only one eruption has been found. The flare frequency was thus derived 0.0376 eruption per hour. Moreover, the hydrogen emission lines are strong indicators of the chromospheric activity (see Fig. 3)

In our photometric campaign, N745 was measured every clear night at Valašské Meziříčí observatory from Jan 22, 2019 to May 26, 2022. Typical light curves obtained in clear filter are plotted in Fig. 8. Altogether 107 observing nights and 594.3 hours of CCD photometry were analyzed. We employed the same flare detection criterion as in our previous study of the active eclipsing binary GJ 3236 (Šmelcer et al. 2017). During this time interval only 6 new eruptions were counted and a new flare frequency of 0.00168 eruption per hour was

Table 9. Parameters of flares observed at Valašské Meziříčí observatory.

No.	Max JD Hel. –2400000	Event	Duration [min]	Amplitude [mag]	Filter
1	59161.56148	Max	4.3	0.13	V
	59161.56223	Max	3.1	0.06	R
2	59309.29322	Max	13.5	0.06	Clear
	59640.45301	Rise	2.5		
3	59640.45301	Max	7.5	0.09	Clear
	59641.26040	Rise	17.0		
4	59641.27220	Max	48.0	0.07	Clear
	59652.59490	Rise	5.2		
5	59652.59853	Max	14.6	0.19	Clear
	59659.58468	Rise	4.0		
6	59659.58468	Max	10.5	0.09	Clear
	59659.58745	Max			

derived. This is 4 times less than was found in the previous study of Zhang et al. (2014).

Detailed information about observed flares are summarized in Table 9. Surprisingly, four eruptions were observed during relatively short time span in March 2022. Having such a small sample, the energies of individual flares were not calculated.

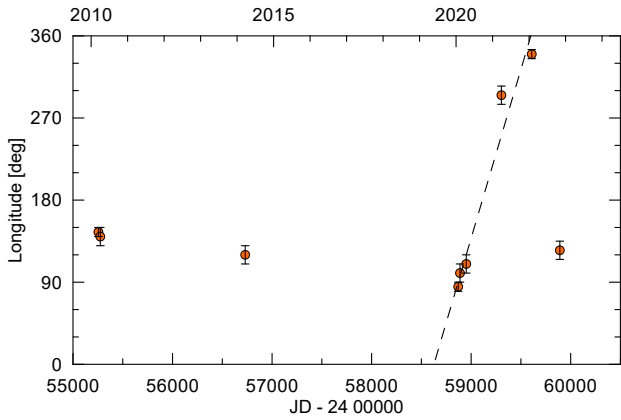


Figure 9. The changes in longitude of the dark structure on the surface of the primary component during several observational epochs. Mean errors in longitude are indicated. The steep dashed line denotes migration of the dark structure during 2020–2022 with the rate about 10 deg/month

6 DISCUSSION

The physical parameters of the binary suggest that the times of the tidal synchronization and orbital circularization are very short. These times can be derived as (Hilditch 2001)

$$t_{\text{sync}} \approx 10^4 \left[\frac{1+q}{2q} \right]^2 P^4, \quad (5)$$

$$t_{\text{circ}} \approx 10^6 q^{-1} \left[\frac{1+q}{2} \right]^{5/3} P^{16/3}, \quad (6)$$

where times are in years, $q = M_2/M_1$ is the mass ratio and P is the orbital period in days. For N745 these times are $t_{\text{sync}} \approx 10^3$ yr and $t_{\text{circ}} \approx 10^5$ yr. These values are very small compared to typical ages of low-mass binaries and justify our assumptions about the orbital circularization and synchronicity parameters.

The seasonal light curves of N745 show slowly evolving and persistent starspot structures that also strongly affect the estimation of precise $O-C$ timings. The apparent period changes are better visible on the run of secondary eclipses and are probably caused by a moving dark structure on the surface of the primary component, where a different part of this region is visible. Position of the dark region derived from available light curves are collected in Table 8. Fig. 9 shows changes in the spot longitude during 12 years including two epochs of TESS photometry. Although the resulting colatitude and the radius of the dark structure remain practically the same, the value of its longitude has been changing over the last few years. This is also well visible on the current $O-C$ diagram (Fig. 5), where secondary minima show a significant shift up to 0.002 days from the predicted values. Due to sparse coverage of this diagram on Fig. 9 we also cannot exclude a rapid change in the longitude of this cold structure found on light curves of N745 during last years 2020–2022. The average migration speed of about 10 deg/month was derived which is close to the value recently derived by Šebek et al. (2022) for another low-mass eclipsing binary V608 Cam.

The sinusoidal changes of the dark region longitude in time were described by Zhang et al. (2014) in another low-mass eclipsing binary system NSVS 2502726. They derived variation with the period 5.9 ± 0.2 yr with an amplitude of about 33 deg. Tran et al. (2013) studied eclipse timing variations in contact binary systems from the

KEPLER archive. They showed that the anticorrelated behavior, the amplitude of the $O-C$ delays, and the overall random walk-like behavior can be explained by the presence of a starspot that is continuously visible around the orbit and slowly changes its longitude on timescales of weeks to months. The quasi-periods of $\sim 50-200$ days were observed in the $O-C$ curves. Later, Balaji et al. (2015) reported rotational motions of spots on the surfaces of components in very short-period, near-contact, and contact binary systems selected from 414 KEPLER light curves. They found that in $\sim 34\%$ of the systems, the spot rotation was retrograde as viewed in the frame rotating with the orbital motion, while $\sim 13\%$ showed significant prograde spot rotation. The remaining systems showed either little spot rotation or erratic behavior, or sometimes include intervals of both types of behavior.

7 CONCLUSIONS

A study of late-type and low-mass binaries provides us with important information about the most common stars in our Galaxy. The next rare system with a large dark region on the surface of the primary component was studied. New ground based and long-term photometric observations of N745 supplemented by the precise TESS photometry were used to determine photometric parameters of the components and to investigate its asymmetric light curve. New mid-eclipse times were determined and up-to date $O-C$ diagram was constructed. The third body orbiting the eclipsing pair announced in our previous study Wolf et al. (2016) was confirmed and more precise LITE elements were obtained. Moreover, our results indicate that N745 is a next quadruple system in an $((1+1)+1)+1$ hierarchy. The detached eclipsing binary is orbiting by a third body with the relatively short period of 425 days only. The fourth body, probably a brown dwarf, has an orbital period of about 12 years.

The $O-C$ diagram assembled on Fig. 4 is one of the most detailed description of the period changes of a low-mass eclipsing binary. Except LITE due to two additional bodies it shows also systematically shifted secondary eclipses caused by surface activity. The longitudinal migration of dark structures on the surface of components is relatively frequent and was studied recently by Yıldız (2021) or Šebek et al. (2022). We can conclude that during years 2020–2022 the motion of the dark structure on the surface of the primary component was prograde and also relatively rapid with the average migration speed of about 10 deg/month.

The third light computed from the light-curve solution (7%) is in good agreement with the value derived from the minimal mass of the third body. The detected very low eruption activity of N745 is remarkable in comparison with similar known low-mass stars.

Long-term systematic monitoring of this object can bring more information about nature of period changes and surface activities. New high-dispersion and high-S/N spectroscopic observations are needed to obtain the radial-velocity curves and to derive accurate masses for this interesting multiple system. It is also a challenge for theoreticians to clarify the origin and dynamical stability of this hierarchical quadruple system with a brown dwarf as the most distant orbiting body.

ACKNOWLEDGMENTS

Useful suggestions and recommendations by an anonymous referee helped us to improve the clarity and correctness of the paper and are greatly appreciated. The research of MW and PZ was partially

supported by the project COOPERATIO - PHYSICS of the Charles University in Prague. HK and KH were supported by the project RVO: 67985815. The authors would also like to thank Lenka Kotková, Ondřejov observatory, Marek Chrastina, Masaryk University Brno, Jan Vraštil, Tereza Jeřábková, and Ondřej Chrenko, all former students of the Charles University in Prague, for their important contribution to photometric observations during past decades.

This paper includes data collected by the TESS mission. Funding for the TESS mission is provided by the NASA Science Mission directorate. Some of the data presented in this paper were obtained from the Mikulski Archive for Space Telescopes (MAST). This work has made use of data from the European Space Agency (ESA) mission GAIA⁷, processed by the GAIA Data Processing and Analysis Consortium (DPAC)⁸. Funding for the DPAC has been provided by national institutions, in particular the institutions participating in the GAIA Multilateral Agreement. This research has made use also of the Keck Observatory Archive (KOA), which is operated by the W.M. Keck Observatory and the NASA Exoplanet Science Institute (NExScI), under contract with the National Aeronautics and Space Administration. This publication makes use of VOSA, developed under the Spanish Virtual Observatory⁹ project funded by MCIN/AEI/10.13039/501100011033/ through grant PID2020-112949GB-I00. VOSA has been partially updated by using funding from the European Union's Horizon 2020 Research and Innovation Programme, under Grant Agreement No. 776403 (EXOPLANETS-A). The following internet-based resources were used in research for this paper: the SIMBAD database operated at CDS, Strasbourg, France, the NASA's Astrophysics Data System Bibliographic Services, and the O-C Gateway of the Czech Astronomical Society.

DATA AVAILABILITY

Some of the data were derived from sources in the public domain, and the respective URLs are provided as footnotes. The other data are available on reasonable request to the authors.

REFERENCES

- Anders F., et al., 2019, *A&A*, **628**, A94
 Applegate J. H., 1992, *ApJ*, **385**, 621
 Bai Y., Liu J., Bai Z., Wang S., Fan D., 2019, *AJ*, **158**, 93
 Balaji B., Croll B., Levine A. M., Rappaport S., 2015, *MNRAS*, **448**, 429
 Bayo A., Rodrigo C., Barrado Y Navascués D., Solano E., Gutiérrez R., Morales-Calderón M., Allard F., 2008, *A&A*, **492**, 277
 Borkovits T., Hajdu T., Sztakovics J., Rappaport S., Levine A., Bíró I. B., Klagyivik P., 2016, *MNRAS*, **455**, 4136
 Chabrier G., Baraffe I., 2000, *ARA&A*, **38**, 337
 Coughlin J. L., Shaw J. S., 2007, *Journal of the Southeastern Association for Research in Astronomy*, **1**, 7
 Dimitrov D. P., Kjurkchieva D. P., 2010, *MNRAS*, **406**, 2559
 Doyle J. G., Butler C. J., van den Oord G. H. J., Kiang T., 1990, *A&A*, **232**, 83
 Eastman J., Siverd R., Gaudi B. S., 2010, *PASP*, **122**, 935
 Frieboes-Conde H., Herczeg T., 1973, *A&AS*, **12**, 1
 Gaia Collaboration 2022, *VizieR Online Data Catalog*, p. I/355
 Gaia Collaboration et al., 2018, *A&A*, **616**, A1
 Gaia Collaboration Brown A. G. A., Vallenari A., Prusti T., de Bruijne J. H. J., Babusiaux C., Biermann M., 2020, arXiv e-prints, p. arXiv:2012.01533

⁷ GAIA, <https://www.cosmos.esa.int/gaia>

⁸ DPAC, <https://www.cosmos.esa.int/web/gaia/dpac/consortium>

⁹ VOSA, <https://svo.cab.inta-csic.es>

- Granzer T., Schüssler M., Caligari P., Strassmeier K. G., 2000, *A&A*, **355**, 1087
 Hilditch R. W., 2001, *An Introduction to Close Binary Stars*
 Irwin J. B., 1952, *ApJ*, **116**, 211
 Irwin J. B., 1959, *AJ*, **64**, 149
 Kim S. L., Chun M. Y., Lee W. B., Doyle L., 1997, *Information Bulletin on Variable Stars*, **4462**, 1
 Kozhevnikova A. V., Svechnikov M. A., Kozhevnikov V. P., 2009, *Astrophysics*, **52**, 512
 Kron G. E., 1950, *AJ*, **55**, 69
 Lacy C. H., 1977, *ApJ*, **218**, 444
 Lucy L. B., 1968, *ApJ*, **151**, 1123
 Mann A. W., Feiden G. A., Gaidos E., Boyajian T., von Braun K., 2015, *ApJ*, **804**, 64
 Mayer P., 1990, *Bulletin of the Astronomical Institutes of Czechoslovakia*, **41**, 231
 McIntyre T., Shaw J. S., 2005, *International Amateur-Professional Photoelectric Photometry Communications*, **101**, 38
 Morales J. C., Gallardo J., Ribas I., Jordi C., Baraffe I., Chabrier G., Vilardell F., 2010, in Prša A., Zejda M., eds, *Astronomical Society of the Pacific Conference Series Vol. 435, Binaries - Key to Comprehension of the Universe*. p. 141
 Morales J. C., Ribas I., Giménez Á., Baroch D., 2022, *Galaxies*, **10**, 98
 Nelson T. E., Caton D. B., 2007, *Information Bulletin on Variable Stars*, **5789**, 1
 Pecaut M. J., Mamajek E. E., 2013, *ApJS*, **208**, 9
 Pettersen B. R., 1989, *Sol. Phys.*, **121**, 299
 Pravec P., Hudec R., Soldán J., Sommer M., Schenk K. H., 1994, *Experimental Astronomy*, **5**, 375
 Prša A., Zwitter T., 2005, *ApJ*, **628**, 426
 Prša A., et al., 2016, *ApJS*, **227**, 29
 Qian S. B., et al., 2012, *MNRAS*, **423**, 3646
 Rappaport S., Deck K., Levine A., Borkovits T., Carter J., El Mellah I., Sanchis-Ojeda R., Kalomeni B., 2013, *ApJ*, **768**, 33
 Ricker G. R., et al., 2015, *Journal of Astronomical Telescopes, Instruments, and Systems*, **1**, 014003
 Shappee B. J., et al., 2014, *ApJ*, **788**, 48
 Stassun K. G., et al., 2019, *AJ*, **158**, 138
 Sterken C., ed. 2005, *The Light-Time Effect in Astrophysics: Causes and cures of the O-C diagram* *Astronomical Society of the Pacific Conference Series Vol. 335*
 Tran K., Levine A., Rappaport S., Borkovits T., Csizmadia S., Kalomeni B., 2013, *ApJ*, **774**, 81
 Vida K., Oláh K., Kóvári Z., Korhonen H., Bartus J., Hurta Z., Posztobányi K., 2009, *A&A*, **504**, 1021
 Wilson R. E., Devinney E. J., 1971, *ApJ*, **166**, 605
 Wolf M., et al., 2016, *A&A*, **587**, A82
 Yoldaş E., 2021, *Rev. Mex. Astron. Astrofis.*, **57**, 351
 Zhang L., Zhang X., Zhu Z., 2010, *New Astron.*, **15**, 362
 Zhang L.-Y., Pi Q.-f., Yang Y.-G., 2014, *MNRAS*, **442**, 2620
 Šebek F., Walter F., Wolf M., 2022, *New Astron.*, **97**, 101879
 Šmelcer L., Wolf M., Kučáková H., Bílek F., Dubovský P., Hoňková K., Vraštil J., 2017, *MNRAS*, **466**, 2542
 van Hamme W., 1993, *AJ*, **106**, 2096

This paper has been typeset from a $\text{\TeX}/\text{\LaTeX}$ file prepared by the author.